Inorganic Chemistry

Article

pubs.acs.org/IC

Methionine Ligand Lability of Homologous Monoheme Cytochromes *c*

Benjamin D. Levin,[†] Kelly A. Walsh,[†] Kristal K. Sullivan,[†] Kara L. Bren,[‡] and Sean J. Elliott*[,†]

[†]Department of Chemistry, Boston University, 590 Commonwealth Avenue, Boston, Massachusetts 02215, United States

[‡]Department of Chemistry, University of Rochester, Rochester, New York 14627, United States

ABSTRACT: Direct electrochemical analysis of adsorbed bacterial monoheme cytochromes *c* has revealed a phenomenological loss of the axial methionine when examined using pyrolytic "edge-plane" graphite (EPG) electrodes. While prior findings have reported that the Met-loss state may be quantitatively understood using the cytochrome *c* from *Hydrogenobacter thermophilus* as a model system, here we demonstrate that the formation of the Met-loss state upon EPG electrodes can be observed for a range of cytochrome orthologs. Through an electrochemical comparison of the wild-type proteins from organisms of varying growth temperature optima, we establish that Met-ligand losses at graphite surfaces have similar energetics to the "foldons" for known protein folding pathways. Furthermore, a downward shift in reduction potential to approximately −100 mV vs standard hydrogen electrode was observed, similar to that of the alkaline transition found in mitochondrial cytochromes *c*. Pourbaix diagrams for the Met-loss forms of each cytochrome, considered here in comparison to mutants where the Met-ligand has been substituted to His or Ala, suggest that the nature of the Met-loss state is distinct from either a His-/aquo- or a bis-His-ligated heme center, yet more closely matches the pK_a values found for bis-His-ligated hemes., We find the propensity for adoption of the Met-loss state in bacterial monoheme cytochromes *c* scales with their overall thermal stability, though not with the specific stability of the Fe−Met bond.

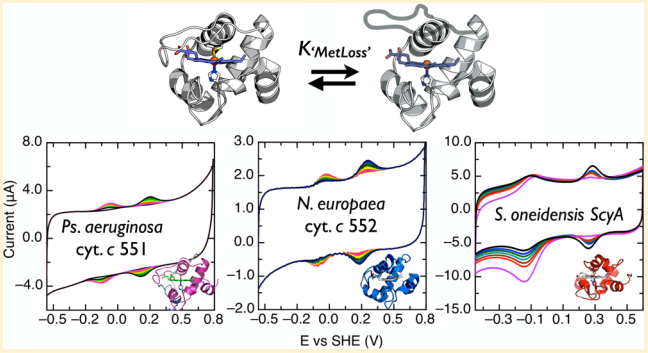

While cytochrome *c* is an important model system for investigation of electron-transfer chemistry and protein folding, we have previously found that canonical His-/Met-ligated cytochromes *c* (cyts *c*) display a propensity for loss of the Met-ligand when examined upon the popular electrode material used in protein electrochemistry, edge-plane graphite (EPG).[1,2] Previously, we have interrogated the Met-loss feature observed in the model system *Hydrogenobacter thermophilus* cytochrome c_{552} (*Ht* cyt c_{552}), finding that when compared to studies conducted on alkanethiol-modified gold, EPG-adsorbed *Ht* cyt c_{552} produces a low-potential, Met-loss state (∼−100 mV vs SHE) susceptible to axial ligand replacement by exogenous small molecules such as imidazole (Im) and that the Im-adduct is similar in reduction potential to the Met-loss feature. The populations of the Met-loss and normal forms of *Ht* cyt c_{552} were found to be reciprocally dependent on temperature, and the redox thermodynamics associated with both forms of the protein were consistent with those from other species.[1] We concluded that interaction with the EPG surface substantially lowers the free energy for the conformational rearrangement of the Met-donating loop for the *Ht* cytochrome.[1] Here, we build upon our previous findings of Met-loss behavior by extending our characterization of bacterial monoheme cytochromes *c*, and we demonstrate that the phenomenon is general to Met-/His-ligated cytochromes *c*. We show that the relative propensity for loss of the Met-ligand can be directly correlated to the global thermal stability of the cyt *c* of interest, though not the apparent stability of the Fe−Met bond alone. Finally, we find that the pK_a values for the $Fe^{(II/III)}$ redox couple for the various Met-loss states are all largely similar, showing a distinct pattern of H^+-coupling that evokes other precedents of bis-His-ligated cyts *c*, yet may not unambiguously implicate a specific misligated state.

Among bacterial class I cytochromes *c* there is a wide variation (>350 mV[3]) in redox potential despite similar protein scaffolds, and here we examine a series of cyts *c* in order to determine the generality of the EPG electrode-induced generation of the Met-loss state. Several mechanisms are implemented to modulate the electronic/redox properties of the heme such as axial ligand identity and orientation, porphyrin ring ruffling, and second sphere interactions.[4] We have chosen to examine a subset of similar cyts *c* with well-characterized redox and structural properties: the cyt c_8 paralogs *Ht* cyt c_{552}, *Pseudomonas aeruginosa* (*Pa*) cyt c_{551}, and *Nitrosomonas europaea* (*Ne*) cyt c_{552}, which have been used as model systems for investigating the impact of protein structure, dynamics, and redox chemistry;[5,6] as well as the ortholog ScyA from *Shewanella oneidensis* (*So*), first purified by Meyer et al.[7] ClustalW2 primary amino acid sequence

Received: May 20, 2014
Published: December 9, 2014

   dx.doi.org/10.1021/ic501186h | *Inorg. Chem.* 2015, 54, 38−46

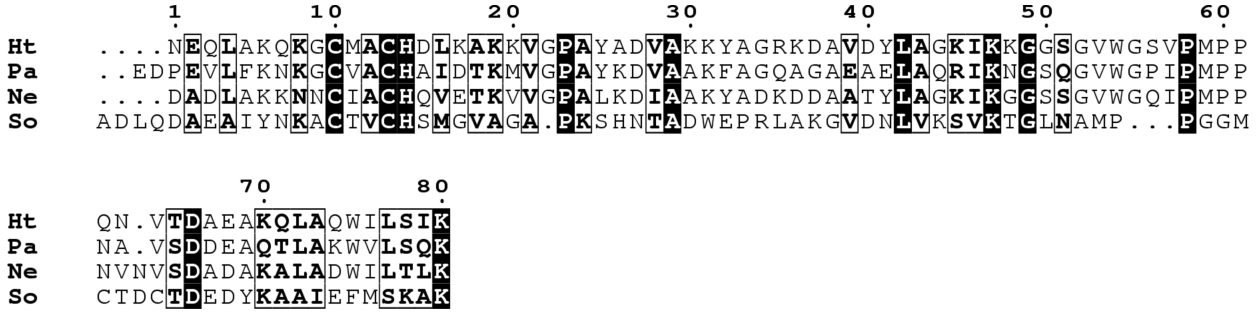

Figure 1. Sequence alignment of monoheme cytochromes *c*. The alignment was carried out with ClustalW2.

alignments are shown in Figure 1, which highlights the overall similarity between these proteins. Table 1 illustrates the structural distinctions between each of the cytochromes considered here, in terms of root mean squared deviation (RMSD) of the backbone of the folded cytochrome.

Table 1. Root Mean Squared Deviation (RMSD) in Angstroms of the Carbon Backbone of the Cytochromes *c* from *Ht* (Protein Data Bank (PDB) 1YNR), *Pa* (PDB 451C), *Ne* (PDB 1A56), and *So* (PDB 1XK7)[a]

	Ht	*Ne*	*Pa*	*So*
Ht	–	–	–	–
Ne	2.013 (60)	–	–	–
Pa	0.471 (56)	2.055 (54)	–	–
So	2.884 (6)	3.233 (18)	7.575 (13)	–

[a]For each entry, the percentage identity between the two primary amino acid sequences is given in parentheses.

Here we investigate the propensity for the loss of the Met-ligand for a series of paralogous cyts *c*, as well as compare the redox thermodynamics of Met-loss form of each protein as observed voltammetrically on EPG electrodes. Ligand binding with imidizaole suggests that, in each case, the Met-loss state involves a displaceable moiety, such as an aquo ligand.[1,2,8] Similarly, investigation of the redox thermodynamics enables the comparison of the principal components of the electrochemical driving force for normal and Met-loss states and further comparison of other cytochromes *c*.[9] Further comparisons of the pH dependence of the redox potential of the Met-loss form of each cyt *c* adsorbed at an EPG electrode suggests that, for all proteins studied here, the Met-loss form is similar, though, with pK_a values, do not unambiguously implicate either a His-/aquo- nor a bis-His-ligated species. Finally, we are able to compare the relative populations of the normal and Met-loss states on the electrode to elucidate the Gibbs free energy for the conformational change.[1] Bolstering these data with the observation of the global unfolding temperatures, and relative stabilities of the Fe-Met bond (inferred via the temperature stability of the Met to Fe charge-transfer band at 695 nm) for each cyt *c* paint a picture where Met-ligand lability occurs readily among monoheme cyts *c* when bound at EPG electrodes. Taken together, we demonstrate an overall correlation between the spontaneity of the conformational transformation and global folding stability.

MATERIALS AND METHODS

Expression and Purfication of Proteins. *So ScyA.* Recombinant *So* ScyA was expressed as was done previously,[10] using plasmid pSOc5 in *Escherichia coli* (*E. coli*) JM109 cells bearing the pEC86 plasmid.[11] Precultures of 10 mL each were grown overnight in 2xYT medium. Large cultures were inoculated with a 1:100 dilution and incubated at 37 °C and 200 rpm, for 22 h. Overexpression was achieved through autoinduction. All media were supplemented with 100 μg/mL ampicillin and 34 μg/mL chloramphenicol. Cell pellets were harvested by centrifugation (6000*g*, 15 min, 4 °C), resuspended in 10 mL/g 20 mM Tris, 1 mM EDTA, 50 mM NaCl, pH 8.0 and 0.1 mg/mL lysozyme, and lysed by sonication. Cell debris was removed by centrifugation. Clarified lysate was adjusted to pH 4.5 by dropwise addition of 1 M acetic acid, and precipitated proteins were removed by centrifugation. The resulting pink supernatant was oxidized by the addition of potassium ferricyanide. Oxidized *So* ScyA was loaded onto MacroPrep High S resin (Bio-Rad) equilibrated in 10 mM sodium acetate, pH 4.5. *So* ScyA eluted over a gradient from 50 to 500 mM NaCl. Eluted fractions around 250 mM NaCl visualize on sodium dodecyl sulfate (SDS) page gels, showing a single band corresponding to approximately 8.5 kDa (calculated MW 8361.51 Da). Fractions with purity ratios (A_{410}/A_{280}) of greater than or equal to 4.0 were pooled and stored in 15% glycerol at −80 °C.

Pa cyt c_{551}. Recombinant *Pa* cyt c_{551} was expressed and purified as described previously.[12] Briefly, the purification of *Pa* cyt c_{551} was conducted by first loading the cleared lysate onto (diethylamino)ethyl (DEAE) resin (GE Healthcare) equilibrated with 10 mM Tris-HCl, pH 7.5. Protein fractions where collected over a 10−40 mM Tris-HCl gradient and concentrated prior to the next purification step. The pH was lowered to below pH 4.0 with acetic acid before loading onto a CM column (GE Healthcare) equilibrated with 10 mM sodium acetate buffer, pH 4.0. The protein is eluted in 10 mM sodium acetate using a pH gradient between 4.0 and 6.0.

Ne cyt c_{552}. pSNEC (Amp^R) was transformed into JM109 *E. coli* harboring the pEC86 (CM^R) containing the cytochrome *c* maturation cassette. Precultures (5 mL) were grown overnight in 2xYT medium. Large cultures were inoculated with a 1:1000 dilution of the preculture and grown for 22 h, at 175 rpm and 37 °C. Cells were harvested by centrifugation (6000*g*, 15 min, 4 °C) and resuspended in 10 mM Tris-HCl, pH 7.0. Cells were disrupted by sonication, and cell debris was removed by centrifugation (10000*g*, 15 min, 4 °C). The cleared supernatant was adjusted to pH 4.6 with 1 M acetic acid and loaded onto high S resin (GE Healthcare) equilibrated with 10 mM sodium acetate, pH 4.5. *Ne* cyt c_{552} was eluted with a 0−180 mM NaCl gradient. The pink fractions were collected, concentrated, and oxidized using potassium ferricyanide. The oxidant was removed using a PD-10 column (GE Healthcare) and was loaded onto MacroPrep High S resin (Bio-Rad) equilibrated in 10 mM sodium acetate, pH 4.5. The protein was eluted with a 0−180 mM NaCl gradient.

Ht cyt c_{552} and Ht M61A and M61H. The *Ht* proteins were produced as described previously.[1]

Electrochemical Methods. All protein film voltammetry (PFV) measurements were carried out on a PGSTAT30 or PGSTAT12 (Ecochemie) electrochemical analyzer equipped with FRA and ECD modules. A three-electrode configuration was used in a water-jacketed electrochemical cell. A resin-body calomel electrode (Accumet) and platinum wire were used as the reference and counter electrodes, respectively. The calomel reference was maintained at a constant temperature (293 ± 0.5 K). Cell temperature was maintained using a

dx.doi.org/10.1021/ic501186h | *Inorg. Chem.* 2015, 54, 38−46

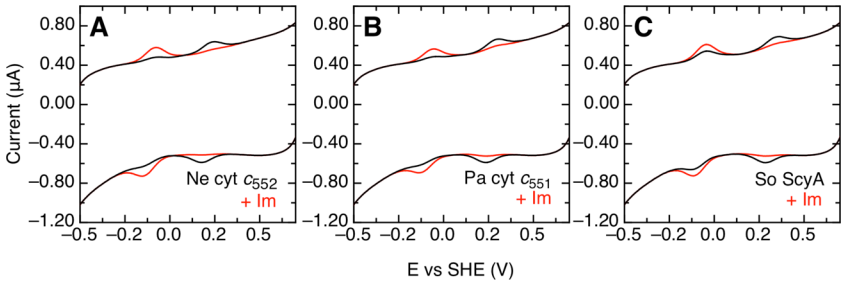

Figure 2. Voltammograms for wild-type (A) *Ne* (B) *Pa*, and (C) *So* cyts *c* in the absence (black) and presence (red) of imidazole (200 mM for the *Ne* and *Pa* proteins, 150 mM for *So* ScyA), measured at 277 K at an EPG electrode.

refrigerating circulator. Pyrolytic edge-plane graphite (EPG), embedded in resin, served as the working electrode for redox thermodynamics and ligand binding studies. EPG electrodes were polished with an aqueous 1 μ alumina slurry, followed by sonication. Protein films were generated by directly applying 2 μL of cyt *c*. Excess protein was washed away with cold buffer. To determine Pourbaix diagrams, the pH of the electrochemical buffer was taken before and after electrochemical analyses. Because the pH dependence of the *So* ScyA protein had not been reported, the His-/Met-ligated form of the protein was examined at 6-mercaptohexanol-modified polycrystalline gold electrodes, as reported previously, in order to compare directly with the *Ht*, *Ne*, and *Pa* cyts *c*.[6]

The redox thermodynamics were examined by PFV as previously described.[1] Electron-transfer thermodynamics was determined by variable-temperature experiments (0−65 °C). Reaction entropy ($\Delta S^{\circ\prime}_{rc}$; rc, redox center) for the $Fe^{(III/II)}$ couple may be determined by the following relation:

$$\Delta S^{\circ\prime}_{rc} = S^{\circ\prime}_{red} - S^{\circ\prime}_{ox} = nF\left(\frac{dE^{\circ\prime}}{dT}\right) \quad (1)$$

$\Delta S^{\circ\prime}_{rc}$ is assumed constant over the temperature range investigated, the slope of E_m vs T should be linear and equal to $\Delta S^{\circ\prime}_{rc}/nF$. From the Gibbs−Helmholtz equation, $\Delta H^{\circ\prime}_{rc}$ may be extracted from the negative slope of an E_m/T vs $1/T$ plot.

The populations of Met-loss and normal forms of each species are determined either as the peak area (total charge passed) for each of the two redox couples or as a quantity proportional to the peak height of each redox couple in a cyclic voltammogram (CV). The peak height formalism for an anodic (oxidation, i_{pa}) or cathodic (reduction, i_{pc}) feature is shown in eq 2.[13]

$$i_p = \frac{n^2F^2A\Gamma v}{4RT} \quad (2)$$

Here, n is the number of electrons, F is the Faraday constant, R is the ideal gas constant, T is the temperature, A is the physical surface area, Γ is the total electroactive coverage, and the scan rate is v. For a process with n equaling unity, the population is directly proportional to the observed current. Temperature-dependent behavior may be assessed using the equilibrium form of the Gibbs free energy equation and linear form of the van't Hoff equation (eq 3):

$$\ln K = -\frac{\Delta H^\circ}{RT} + \frac{\Delta S^\circ}{R} \quad (3)$$

The equilibrium constant K_{eq} may be determined at each temperature by the ratio of Met-loss to normal form, and a plot of $\ln(K_{eq})$ vs T^{-1} allows the extraction of the thermodynamic parameters. Here we assessed K_{eq} in terms of the peak height of each redox couple. ΔG° values were calculated at 298 K.

Circular Dichroism and Thermal Denaturation. Circular dichroism (CD) spectroscopy was performed on an Applied Photophysics CS/2 Chirascan spectrophotometer equipped with a CD 250/AP temperature-controlled cuvette holder (Quantum Northwest) and controlled with a TC125 temperature controller (Quantum Northwest). Measurements were conducted with a 0.10 cm path length two-piece quartz cell (Starna). All experiments used 50 μM protein. CD spectra were collected with a window of 180−280 nm, an averaging time of 1 s, and a bandwidth of 1 nm. Thermal unfolding was monitored as either a continuous-ramp experiment at 0.5 °C min^{-1} or as a step ramp with 2 °C steps and 2 min equilibration time at each temperature over 10−92 °C. Reversibility of samples without denaturant was determined by return of the temperature to 10 °C, collection of a final CD spectrum, and verification that the spectrum is the same as that of the starting material.

Guanidine hydrochloride (GuHCl) was used for denaturation experiments. A fresh stock solution of GuHCl (Sigma) was used and diluted in 5 mM MES, pH 7.0. The pH of each protein solution was adjusted with a small amount of sodium hydroxide to pH 7.0. The ionic strength of each sample was maintained at 1.25 M with sodium sulfate. Unfolding was monitored using a step-ramping experiment as described previously with GuHCl ranging from 0.25 to 1.25 M. Reversibility was determined by removing the denaturant and verifying the CD spectra of each protein sample. Spectra were collected from 180 to 280 nm as described earlier; however, below 200 nm the spectra are distorted due to the presence of GuHCl and will only be displayed in the wavelength range of 200−280 nm.

Data analysis was done by determining the fraction folded (α) at any given temperature by processing the change in ellipticity at 222 nm (eq 4).[14]

$$\alpha = \frac{\theta_t - \theta_F}{\theta_F - \theta_U} \quad (4)$$

The parameters of eq 4 are the observed ellipticity at a given temperature (θ_t) and for the fully folded (θ_F) and the fully unfolded (θ_U) proteins. The thermal unfolding temperature (T_m) is determined when $\alpha = 0.5$. Determining the T_m at zero denaturant was done using a linear extrapolation method by plotting T_m vs [GuHCl].[6,14]

RESULTS

As previously reported[1,2,5] all of the cyts *c* yielded excellent electrochemical responses when adsorbed onto EPG electrodes. Similar to our prior results with *Ht* cyt c_{552}, *Ne* cyt c_{552}, *Pa* cyt c_{551}, and *So* ScyA all exhibited a reversible redox couple at high potential (~200 mV) evocative of the His-/Met-ligated heme center, as well as a lower potential (~−100 mV) "Met-loss" form that could be observed to lesser or greater extents (Figure 2). To assess if the Met-loss form of each cyt *c* contains a potentially labile ligand, imidazole (Im) was added to the cell solution, which induced a modulation of the PFV response in all cases (Figure 2, red traces): nearly the entire population of the His-/Met-ligated cyt *c* disappeared, and the apparent electrocoverage of a low-potential form of cyt *c* grew; with the increase of a low-potential species is presumed to be an Im-adduct of similar, though nonidentical, potential (Table 2).

Proton Dependence of Met-Loss Electrochemistry. Figure 1 clearly demonstrates that, for the *Ne*, *Pa*, and *So* cytochromes, the Met-loss form of the protein can be generated

dx.doi.org/10.1021/ic501186h | Inorg. Chem. 2015, 54, 38−46

Table 2. Midpoint Potentials Determined for the Normal and Imidizole-Bound Adducts of Homologous Cytochromes *c*, pH 6.0[a]

	E_m vs SHE (mV)	
cyt *c*	normal	+Im
So	313 ± 3	−76 ± 3
Pa	277 ± 3	−89 ± 2
Ht[1]	210 ± 2	−110 ± 3
Ne	205 ± 2	−111 ± 2

[a]Data for *Ht* cyt c_{552} taken from ref 1.

in a fashion similar to that of *Ht* cyt c_{552}. To better establish the possible identity of the electrochemically detected low-potential form of each cytochrome, we further compared the pH dependence of the redox potential of Met-loss states observed, to examine potential proton-coupling events that might be attributed to a novel ligand such as His/Lys/H_2O that could bind at the heme center in the presumed absence of the Met-ligand. The Pourbaix diagram for the redox chemistry of the Met-loss form of the *Ht*, *Ne*, and *So* cytochromes are shown in Figure 3A, along with data for the *Ht* M61A and M61H mutants, where it can be presumed that, at the EPG electrode, aquo and His are bound as ligands, respectively. Remarkably, all three Met-loss states show a highly similar pH dependence, easily modeled by a single pK_a for the oxidized and reduced forms of the protein. Here, pK_{ox} and pK_{red} values are easily separated for each Met-loss state (4.9 and 8.1 for *Ht*, 5.4 and 7.6 for *Ne*, and 5.4 and 7.4 for *So*, respectively), indicating that a single proton is coupled to electron-transfer steps at the heme center around neutral pH. In contrast, neither *Ht* mutant demonstrated a significant pH dependence (Figure 3A, green and open triangles). Figure 3B compares the pH dependence of the redox potentials of the His/Met versions of the cyts *c* studied here, where previously determined proton-coupling has been established for *Pa*, *Ne*, and *Ht* cyts *c*[6] and are compared to *So* ScyA, which shows a nominal pH dependence, that cannot be described by a simple $1H^+$:$1e^-$ scheme. Thus, the nature of the proton-coupling for each Met-loss state does not appear to directly correlate to the proton-coupling scheme of the His-/Met-ligated forms of the parent, native cytochrome.

Redox Thermodynamics. Variable-temperature electrochemistry was used to elucidate the thermodynamic parameters, $\Delta H^{\circ\prime}_{rc}$ and $\Delta S^{\circ\prime}_{rc}$, that contribute to the Gibbs free energy of the redox reaction (where rc indicates the redox center). Figure 4 illustrates the impact of temperature upon the voltammetry of the *Pa*, *Ne*, and *So* cytochromes. The case of *So* ScyA (Figure 4A) is typical: over a range of temperatures (273−288 K) increasing temperature reversibly minimized the appearance of the typical His-/Met-ligated cyt *c* and maximized the population of the Met-loss state.

For all of the cytochromes studied, over the temperature range where the protein would adsorb, the redox potential follows a linear trend. The temperature dependences of the reduction potential for both normal and Met-loss (ML) forms are plotted along with the corresponding Gibbs−Helmholtz plots for *So* ScyA, *Pa* cyt c_{551}, and *Ne* cyt c_{552} (Figure 5). In each case the change in redox potential is linear with respect to temperature, suggesting that only one species exists for each redox couple. Analysis of the redox thermodynamics for both the His-/Met-ligated and Met-loss forms of the *Pa*, *Ne*, and *So* cyts *c* are summarized in Table 3.

In behavior similar to that observed previously for *Ht* cyt c_{552}, the current magnitude of the two redox couples (Figure 4) changed reversibly as a function of temperature, in all cases. As the temperature was increased, a loss of the His-/Met-ligated form occurred with a proportional increase in the Met-loss feature. The electrochemical area or peak current conveys the relative amounts of each redox active species on the electrode.[1] From those data the equilibrium constant for the conformational change ($K_{eq,ML}$) between the native Met-bound and Met-loss states was extracted and expressed in terms of a free energy, ΔG_{ML}, as discussed later.

Cytochrome *c* Stability. Thermal denaturation monitored by circular dichroism was used to evaluate the relative stability of *Ne* cyt c_{552} and *So* ScyA with respect to the reported values for *Pa* and *Ht* cyt *c*.[6] Importantly, this allowed the evaluation of the relative stability of these cytochromes with respect to the observed Met-loss feature and conformational plasticity. Melting studies were performed in the absence of denaturant for *So* ScyA, with spectra that were collected in both continuous-ramp and step-gradient modes. Both methods reproducibly resulted in a T_m = 66 °C, with an average deviation in observed melting temperature of 0.3 °C (Figure 6).

All of the cyt *c* data were collected in the step-gradient mode but were complicated by the overall stability of the protein

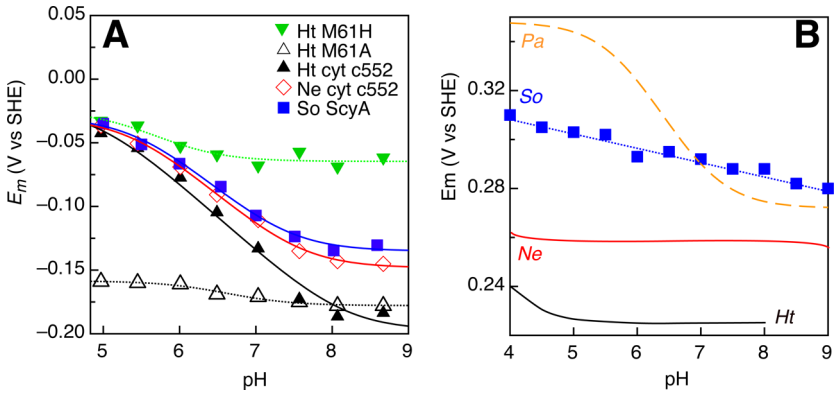

Figure 3. (A) pH dependence of the Met-loss forms of *Ht*, *Ne*, and *So* cyts *c*, compared to the *Ht* M61A and M61H mutants at EPG electrodes. Data were fit to a simple $1H^+$:$1e^-$ model as in ref 6. Data for *Pa* cyt c_{551} is superimposable to that for the Met-loss form of wild-type *Ht* cyt c_{552} and is omitted for clarity. (B) pH dependence of the His-/Met-ligated *So* ScyA reduction potentials at 6-mercaptohexanol-modified gold electrodes and compared to *Pa*, *Ne*, and *Ht* orthologs (data taken from ref 6).

dx.doi.org/10.1021/ic501186h | *Inorg. Chem.* 2015, 54, 38−46

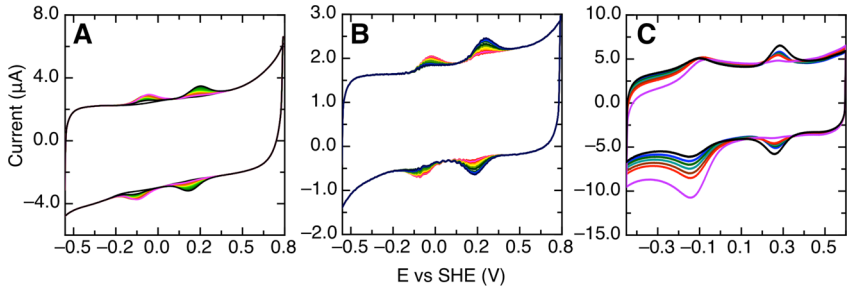

Figure 4. Variable-temperature PFV response of (A) *Ne* cyt c_{552}, (B) *Pa* cyt c_{551}, and (C) *So* ScyA at an EPG electrode. The film was generated at 273 K (black). Subsequently, the temperature was steadily warmed linearly to 275.5 (blue), 278 (light blue), 280.5 (teal), 283 (brown), 285.5 (red), and 288 K (pink). All data were collected at pH 7.0.

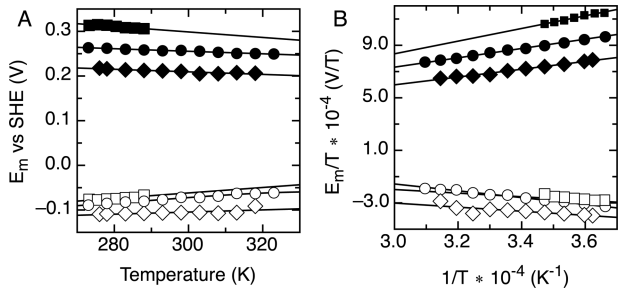

Figure 5. (A) Temperature dependence of E_m determined at EPG electrodes and (B) Gibbs–Helmholtz plot for *So* ScyA ((filled squares) His/Met and (open squares) Met-loss), *Ne* cyt c_{552} ((filled diamonds) His/Met and (open diamonds) Met-loss), and *Pa* cyt c_{551} ((filled circles) His/Met and (open circles) Met-loss). The data were fit to a linear regression model (solid lines).

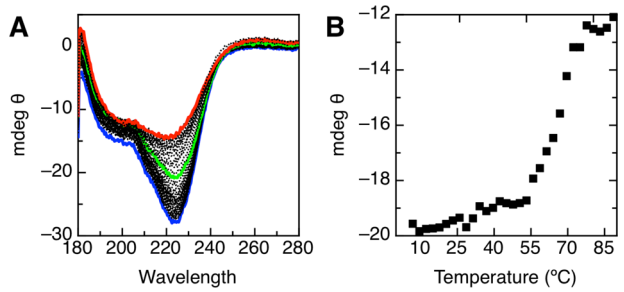

Figure 6. (A) Representative CD spectra of *So* SycA highlighting 10 (blue), 66 (green), and 92 °C (red), and (B) extracted ellipticity at 222 nm for 50 μM *So* ScyA from 10 to 92 °C (with 5 mM MES and 10 mM NaCl, pH 7.0).

(near the thermal limit of the instrument used). *Ne* cyt *c* was too stable to acquire a full melting curve in the absence of denaturant (Figure 7). Here we repeated the melting experiment in the presence of varying amounts of GuHCl (Figure 6B), after which we extrapolated to zero GuHCl using the linear extrapolation method (Figure 6C).[14] The overall shapes of the CD spectra are similar between *So* and *Ne* proteins and are typical for α-helical proteins;[14] however, the dip at 222 nm is much more pronounced for *So* ScyA (Figure 6A) than for *Ne* cyt c_{552} (Figure 7) despite their overall structural similarity (Table 1).

Finally, the specific stability of the Fe–Met bond was examined in terms of the thermal stability of an optical band at 695 nm, attributed to a Met–Fe interaction.[15,16] In contrast to differences in global thermal stability as determined by CD, the optical monitoring of the A_{695} absorption revealed that the *So* and *Ne* proteins are nearly identical in behavior, and are signficinatly lower in terms of the apparent stability of their Fe–Met bond, when compared to prior data for the *Ht* and *Pa* cytochromes, Figure 8.

DISCUSSION

Previously we have detected a so-called Met-loss form of three cyts *c* at graphite electrodes[2] common in the field of protein electrochemistry,[13] and we have further assessed the redox thermodynamics of this novel state in the context of the hyperthermophilic *Ht* cyt c_{552}.[1] Here, we have extended these findings, by both interrogating the nature of the Met-loss state and demonstrating the generality of the conformational change (and the energetics thereof) as monoheme cyts *c* interact with EPG electrodes.

To better explicate the surface-induced electrochemical phenomena, we chose to examine two cyts *c* that are closely related to *Ht* cyt c_{552}, *Pa* cyt c_{551}, and *Ne* cyt c_{552}, and the more distantly related *So* ScyA cytochrome.. The *Ht*, *Pa*, and *Ne* cyts *c* are all members of the cytochrome c_8 structural family[17] and all have been studied previously as model systems for examining the interplay between protein folding, structural stability, and redox function.[2,5,6,18–20] Notably, these three

Table 3. Thermodynamic Parameters Determined by Protein Film Voltammetry for the Normal and Met-Loss Forms of Various Bacterial Cytochromes *c*

protein	$\Delta S^{\circ\prime}_{rc}$ (J K^{-1} mol^{-1})	$\Delta H^{\circ\prime}_{rc}$ (kJ mol^{-1})	$\Delta S^{\circ\prime}_{ML}$ [b] (J K^{-1} mol^{-1})	$\Delta H^{\circ\prime}_{ML}$ [b] (kJ mol^{-1})	ref
Ht wt	−49.1	−42.2	95.7	36.7	1
Ht M61H	−127	−31.1			1
Ht M61A	−56.2	−3.7			1
Pa	−28.9	−32.9	57.9	23.6	this study
Ne	−67.5	−37.16	19.3	18.4	this study
So	−57.9	−46.5	57.9	23.4	this study

[a]The average errors for $\Delta S^{\circ\prime}$ and $\Delta H^{\circ\prime}$ are ±4 J K^{-1} mol^{-1} and ±3 kJ mol^{-1}respectively. [b]Met-Loss form.

dx.doi.org/10.1021/ic501186h | *Inorg. Chem.* 2015, 54, 38–46

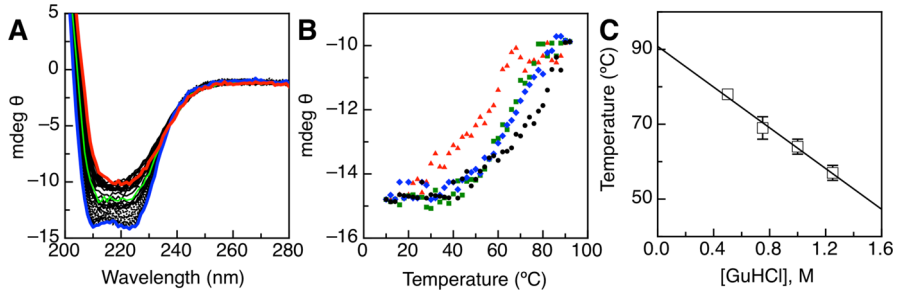

Figure 7. (A) Representative CD spectra of *Ne* cyt *c* in the presence of 1.25 M GuHCl highlighting 10 (blue), 54 (green), and 92 °C (red). (B) Thermal unfolding curves for *Ne* cyt *c* in the presence of (red triangles) 1.25 M, (green squares) 1 M, (blue diamonds) 0.75 M, and (black filled circles) 0.5 M GuHCl. Samples were in 5 mM MES, pH 7.0, with GuHCl and Na_2SO_4 to make the total ionic strength 1.25 M. Collected in step-ramp mode of 2 °C steps with 2 min equilibration time, 1 s averaging, and 1 nm bandwidth. (C) Plots of T_m as a function of [GuHCl] for *Ne* cyt *c*.

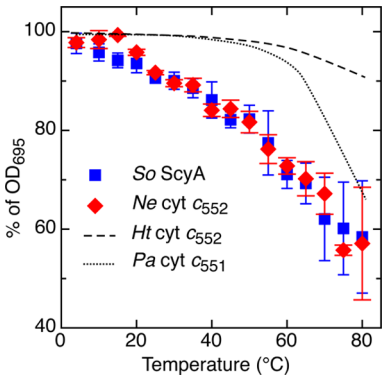

Figure 8. Percent intensity for the 695 nm absorption band for *So* ScyA and *Ne* cyt c_{552}, compared to data for the *Pa* and *Ht* orthologs from ref 16.

cytochromes differ in the electronic structures of their heme environments, which manifests in differences in previously reported redox potentials measured at alkanethiol-modified gold electrodes (recapitulated in Figure 3B), and in distinct proton dependencies.[5] At least some of the difference in redox potential has been ascribed to the environment associated with the axial Met-ligand, which can be "fluxional" (sampling between *R* and *S* conformations) in the case of the *Ne* and *Ht* cyts *c*[21,22] and is static in the case of the *Pa* protein. In contrast, *So* ScyA was chosen to provide a distantly related bacterial cyt *c*, as it shares between 6 and 18% sequence identity to the cyt c_8 family members in our study (Table 1). The equivalent appreciation of electronic structure and redox properties of *So* ScyA has proven much less clear: the solution structure of *So* ScyA reveals no analogous residue to Asn 64 in *Pa* that could enforce a single Met conformation, yet specific fluxional behavior of the Met was not reported.[23] However, regardless of the fluxional status of the Met-ligand, loss of the Met-ligand can occur on EPG electrodes readily and the possibility of fluxionality does not correlate with either apparent Fe−Met bond stability (Figure 7) or the global protein stability.

Thus, whether comparing paralogs with a higher or lower percentage identity, the interconversion between His-/Met-ligated heme environment and a Met-loss state can be readily and reversibly achieved at EPG electrodes, yet the description of the heme center (spin state, coordination number) is not directly apparent from the electrochemistry alone. Surface-based spectroscopies (e.g., Raman) have been employed on gold-based electrode materials and would therefore suggest a possible tool for examining the nature of the Met-loss state(s) in more detail. However, such methods have yet to be established on the rough graphite materials used and elsewhere in the protein electrochemistry literature. In the following sections, we first consider the potential nature of the Met-loss state, as can be suggested from comparisons between wild-type cytochromes and mutants of the well-studied *Ht* cyt c_{552}, and then examine the energetics associate with its formation. As discussed later, the relative propensity for loss of the Met-ligand at EPG electrodes appears to correlate to the overall folding energetics suggesting that generation of the Met-loss state may require larger length-scale perturbations of structure aside from a single Met-donating loop.

Assessing the Identity of the Met-Loss State. As all of the cyts *c* studied here display a population of a Met-loss state upon EPG electrodes, the Met-loss state can be converted to a presumed His-/Im-bound state through the addition of imidazole (Figure 2). Notably, the redox potential of the Im-adducts are not identical, becoming more positive as the sequence identity decreases from that of *Ht* cyt c_{552}, suggesting that the Met-loss form of the protein has a readily exchangeable ligand $Fe^{(II/III)}$, whereas the overall voltammetric reversibility of the Im-bound form of the cytochrome indicates that the complex must be stable when either ferric or ferrous. In general, the slight positive shift in redox potential for the Im-bound adducts (compared to the Met-loss state in Table 2) is expected, whether considering the Im−Fe interaction to serve as a model for a Lys−Fe or a His−Fe interaction:[24,25] a positive shift in the redox potential upon Im-binding has been observed for microperoxidase previously,[8,26]

To further elucidate the potential identity of the Met-loss state, we examined the Pourbaix diagrams for the Met-loss forms of the cytochromes studied here and compared them to data for wild-type *Ht* cyt c_{552} and *Ht* mutants where the Met-ligand has been mutated to either His or an Ala, providing models where only the sixth, axial ligand is thought to change. Surprisingly, all Met-loss forms for wild-type proteins show simple Pourbaix diagrams that are easily modeled by coupling to a single protonation event (in fact, the *Pa* protein gives data[2] nearly exactly matching the *Ht* system and is omitted for clarity). Here, the shape of the Pourbaix diagram more closely resembles either the Met61His mutant of *Pa* cyt c_{551},[27] or the natively bis-His-ligated cyt c_{552} from *Thermosynechococcus elongatus* (*T. elongatus*),[28] where both cases show a pH dependence with two distinct, well-separated pK_as. Considering the Pourbaix diagram of known His-/aquo-ligated hemoproteins, myeloperoxidase displays essentially no pH dependence from pH 4 to 8 in the presence of chloride-containing buffers.[29] To our knowledge, a full Pourbaix diagram for MP8-

dx.doi.org/10.1021/ic501186h | *Inorg. Chem.* 2015, 54, 38−46

microperoxidase has yet to be determined, yet the aquo/hydroxyl pK_a values have been measured for the oxidized and reduced hemes (9.6 and 10.2, respectively), suggesting that the potential will not vary as a function of pH close to neutral pH values, unlike the Met-loss state.

However, when further investigating if the pH-dependent behavior of the Met-loss potentials can distinguish between bis-His or His-/aquo-ligation, we compared the Met-loss state to the *Ht* M61H and M61A mutants (which possess bis-His and His-/aquo-ligation, respectively). In both cases the observation of proton-coupling disappears (Figure 3A), and neither the M61H mutant nor the M61A Pourbaix diagram mimics the Met-loss state, instead evoking the overall shape of the native His-/Met-ligated *Ht* protein (Figure 3B).

Taken together, the Pourbaix data cannot be used to implicate one heme state unequivocally, though it more closely matches bis-His-ligated cyts *c*. It is clear that generation of the Met-loss state should not be thought of as a simple loss of Met as a ligand and subsequent substitution of a non-Met-ligand, as neither *Ht* mutant recapitulates the shape of the Met-loss Pourbaix diagram. As discussed later, we consider the reorganization of each cyt *c* heme environment at EPG to be significant and suggest that the distinction between the M61H data and the apparent bis-His nature of the Met-loss data stems from further conformational changes that occur in proximity to the heme center.

Redox Thermodynamics and Met-Loss Equilibrium. Summarized in Table 3, the redox thermodynamics of the *Pa*, *Ne*, and *So* cyts *c* reveal that, like the *Ht* cytochrome, the His-/Met-ligated form reveals negatively signed enthalpic and entropic terms for the $Fe^{(III/II)}$ redox reaction, while the Met-loss state (in all cases) shows thermodynamic parameters of positive magnitude. None of these bacterial cyts *c* have the break in the E_m vs T (Figure 5A) or Gibbs−Helmholtz plots (Figure 5B) that has been shown for many mitochondrial species,[8,26] indicating, for both the His/Met and Met-loss forms, just two states can be considered in their redox reactions over the temperatures considered here. With respect to the actual magntitudes of $\Delta(H^\circ_{rc})'$ and $\Delta(S^\circ_{rc})'$, the values compare well with both mitochondrial cyt *c* and microperoxidases,[8,30,31] where Sola and co-workers showed that enthalpic and entropic terms are largely compensative due to solvation and axial ligation.[8] Comparison between the entropic and enthalpic terms show that the driving force between the normal and Met-loss forms is largely dictated by the enthalpic term; the redox enthalpy has been largely correlated with the stabilization of the $Fe^{(II)}$ state. We note, however, for the Met-loss forms the magnitude of $\Delta(H^\circ_{ML})'$ alone does not correlate with the observed stability of the Fe−Met interaction, as observed through the thermal stability of the A_{695nm} absorption feature (Figure 8). For example, comparison of the $\Delta(H^\circ_{ML})'$ values alone would suggest that the *So* ScyA protein (24.4 kJ/mol) would be as stable as the *Pa* cyt c_{551} (23.6 kJ/mol), yet Figure 8 clearly shows that the *So* ScyA does not have as robust an Fe−Met interaction

As a consequence of examining both adsorbed species simultaneously, we are able to simultaneously measure the populations of the native and Met-loss forms. The populations are directly proportional to the peak height and/or the total current passed for each redox couple (peak area). We were able to use these values to calculate an equilibrium constant describing the conversion of the normal form to Met-loss, K_{ML}. Plotting $\ln(K_{ML})$ vs T^{-1} (Figure 9) yields a slope of

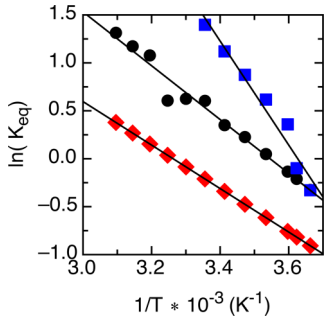

Figure 9. Plot of $\ln(K_{eq})$ vs T^{-1} used to determine the Gibbs free energy for the conversion of the His-/Met-ligated cytochromes at EPG electrodes. The equilibrium constant (K_{eq}) was determined for *So* ScyA (squares), *Pa* cyt c_{551} (circles), and *Ne* cyt c_{552} (diamonds). Linear regression analysis was used to fit each data set and is shown by the solid lines.

$-\Delta H^\circ_{Met\text{-}loss}/R$ and a *y*-intercept of $\Delta S^\circ_{Met\text{-}loss}/R$, where the thermodynamic terms correspond to the specific reorganization of the Met/His to Met-loss form of each cytochrome at the electrode (Table 4) The enthalpy for the conversion is within the regime for subglobal free energies of hydrogen exchange (ΔG_{HX}) and those determined by direct voltammetry (ΔG_{AT}), and here, in all cases the entropic contribution to the overall free energy of the conversion is substantial. As with considering $\Delta(H^\circ_{ML})'$, if we consider the enthalpic contribution to the Met-loss reaction ($\Delta H^\circ_{Met\text{-}loss}$), the values alone do not scale with the observed stabilities of the Fe−Met interaction observed optically: again *So* ScyA appears to have an enthalpic term more like the *Ht* protein, and less like the *Ne* case, which it closely resembles in terms of Fe−Met thermal stability. Thus, $\Delta H^\circ_{Met\text{-}loss}$ likely includes information regarding the specific strength of the Fe−Met bond; the bond-breaking does not account for the enthalpic term alone.

Table 4 also places these data within the context of free energies associated with other cytochrome *c* folding units, termed foldons, including those from horse heart (*Hh*) and yeast (YCC), where ΔG values for foldons have been determined by hydrogen−deuterium exchange (ΔG_{HX}) or for bulk voltammetry (ΔG_{AT}). Regardless, the interaction of bacterial cyts with EPG surfaces appears to lower the free energy requirements to lose the axial methionine ligand.

The thermal melting study has revealed a notable correlation between overall thermal stability of the protein (as measured by T_m) and the propensity for loss of the Met-ligand (Table 4). Those members of the class I family that adopt the Met-loss conformation at higher temperatures are also more stable as measured by T_m. Furthermore, the conformational plasticity also appears to be correlated with optimal growth temperature, with the sole exception of *Ne*. In general, protein thermostability in an organism tends to track with growth temperature.[35] *Ht* is a thermophile originating from Japanese hot springs.[36] *Pa* is a mesophile: *Pseudomonas aeruginosa* is a common soil bacterium that in pathogenic strains thrives at host temperatures (~37 °C).[37] *So* grows optimally at room temperature and with a maximum temperature of approximately 35 °C.[38]

The biological purpose of alternate conformations of His-/Met-ligated cytochromes *c* is an area of renewed interest, particularly with respect to the connection between loss of the Met-ligand and the generation of forms of cyt *c* that can lead to peroxidase activity in mitochondrial cyt *c*. It is clear that

dx.doi.org/10.1021/ic501186h | Inorg. Chem. 2015, 54, 38−46

Table 4. Comparison of Gibbs Free Energy for the Met-Loss Conversion (ML), Subglobal Hydrogen Exchange of the Methionine-Donating Loop (HX), and Mitochondrial Cytochrome *c* Alkaline Form (AT) Where a Nitrogenous Base Has Replaced the Met-Ligand[a]

species	$\Delta S_{\text{Met-loss}}$ (J K^{-1} mol^{-1})	$\Delta H_{\text{Met-loss}}$ (kJ mol^{-1})	$\Delta G_{\text{ML,298K}}$ (kJ mol^{-1})	ΔG_{HX} (kJ mol^{-1})	ΔG_{AT} (kJ mol^{-1})	T_m (°C)
Ht cyt c_{552}	103.0	37.0	6.3[1]			139[6]
Ne cyt c_{552}	54.0	18.8	2.7			91 ± 3
Pa cyt c_{551}	86.1	23.3	−2.3	26−34[32]		80[6]
So ScyA	174.6	45.1	−6.9			66 ± 4
Hh cyt *c*				26.3[33]		
beef heart cyt *c*					52[34]	
YCC					48[30]	

[a]Uncertainties for $\Delta S^{\circ}_{\text{Met-loss}}$, $\Delta H^{\circ}_{\text{Met-loss}}$, and ΔG_{ML} are ±4 J K^{-1} mol^{-1}, ±1.5 kJ mol^{-1}, and ±2 kJ mol^{-1}, respectively.

interactions between mitochondrial cyt *c* with membranes, as suggested here by the interaction with graphitic edge electrodes, lead to cytoplasmic relocation during apoptosis,[39] and that specific unfolding and generation of peroxidase activity have been associated with the binding of the lipid cardiolipin.[40,41] Most recent efforts by Pletneva and co-workers have emphasized the distinct populations of folds associated with peroxidase activity due to lipid−cyt *c* interactions, demonstrated through fluorescence resonance energy transfer (FRET) measurements.[42] Further it has been demonstrated that individual mutations of human mitochondrial cyt *c* decrease the pK_a for the structural rearrangement to the alkaline conformation, and as a consequence the ability to activate apoptotic protease activating factor 1 (Apaf-1) is enhanced.[43] Here, where specific structural information may not be available, it is clear from the direct electrochemical readout that loss of the Met-ligand can be found throughout a range of Met-/His-ligated monoheme cyts *c* and that the free energy associated with that transformation (when the cyt *c* is noncovalently bound to a surface) is small—even being favorable in the case of proteins with a sufficiently low thermal stability of folding.

CONCLUSION

In conclusion, we have shown that the axial ligand of homologous cytochromes *c* from *Shewanella oneidensis*, *Nitrosomonas europaea*, and *Pseudomonas aeruginosa* can be readily perturbed at EPG electrodes common to the field of protein electrochemistry. Comparison of these "Met-loss" states in a side-by-side fashion to the established *Hydrogenobacter* ortholog and its mutants does not lead to a clear picture of the identity of the ligands at the heme center in the Met-loss state. The pH dependence of the Met-loss form is not perfectly modeled by either *Ht* M61H (bis-His) or *Ht* M61A (His/aquo coordination environment), yet displays well-separated pK_{ox} and pK_{red} values, such as other known bis-His-ligated cytochromes. . There is correlation between overall folding stability (and not the specific thermal stability of the Fe−Met interaction) and the propensity to adopt the electrochemically detected Met-loss form. While the identity of the coordination environment within the Met-loss state of each cytochrome is not resolved, it is clear that the required driving force for the rearrangement from normal to the Met-loss form is enhanced by the presence of the EPG surface, and involves relatively small free energy changes, suggestive of a role for other intermolecular interactions in localized unfolding of cytochromes *c*.

AUTHOR INFORMATION

Corresponding Author

*E-mail: elliott@bu.edu. Tel.: 617-358-2816. Fax: 617-353-6466.

Notes

The authors declare no competing financial interest.

ACKNOWLEDGMENTS

We gratefully acknowledge the generous support of the National Science Foundation (Grants MCB546323, CHE1310012, and CHE1126545). S.J.E. thanks Prof. Mookie Baik for stimulating discussions regarding the work presented here.

REFERENCES

(1) Levin, B. D.; Can, M.; Bowman, S. E. J.; Bren, K. L.; Elliott, S. J. *J. Phys. Chem. B* **2011**, *115*, 11718−11726.
(2) Ye, T.; Kaur, R.; Senguen, F. T.; Michel, L. V.; Bren, K. L.; Elliott, S. J. *J. Am. Chem. Soc.* **2008**, *130*, 6682−6683.
(3) Reedy, C. J.; Gibney, B. R. *Chem. Rev.* **2004**, *104*, 617−649.
(4) Bowman, S. E. J.; Bren, K. L. *Development of spectroscopic probes of second-sphere interactions in cytochromes c*; University of Rochester: Rochester, NY, USA, 2010.
(5) Ye, T.; Kaur, R.; Wen, X.; Bren, K. L.; Elliott, S. J. *Inorg. Chem.* **2005**, *44*, 8999−9006.
(6) Wen, X.; Patel, K. M.; Russell, B. S.; Bren, K. L. *Biochemistry* **2007**, *46*, 2537−2544.
(7) Meyer, T. E.; Tsapin, A. I.; Vandenberghe, I.; De Smet, L.; Frishman, D.; Nealson, K. H.; Cusanovich, M. A.; Van Beeumen, J. J. *OMICS: J. Integr. Biol.* **2004**, *8*, 57−77.
(8) Battistuzzi, G.; Borsari, M.; Cowan, J. A.; Ranieri, A.; Sola, M. *J. Am. Chem. Soc.* **2002**, *124*, 5315−5324.
(9) Battistuzzi, G.; Borsari, M.; Sola, M. *Antioxid. Redox Signaling* **2001**, *3*, 279−291.
(10) Pulcu, G. S.; Frato, K. E.; Gupta, R.; Hsu, H.-R.; Levine, G. A.; Hendrich, M. P.; Elliott, S. J. *Biochemistry* **2012**, *51*, 974−985.
(11) Arslan, E.; Schulz, H.; Zufferey, R.; Kunzler, P.; Thony-Meyer, L. *Biochem. Biophys. Res. Commun.* **1998**, *251*, 744−747.
(12) Cutruzzola, F.; Ciabatti, I.; Rolli, G.; Falcinelli, S.; Arese, M.; Ranghino, G.; Anselmino, A.; Zennaro, E.; Silvestrini, M. C. *Biochem. J.* **1997**, *322* (Pt 1), 35−42.
(13) Leger, C.; Bertrand, P. *Chem. Rev.* **2008**, *108*, 2379−2438.
(14) Greenfield, N. J. *Nat. Protoc.* **2006**, *1*, 2733−2741.
(15) Schejter, A.; George, P. *Biochemistry* **1964**, *3*, 1045−1049.
(16) Yamamoto, Y.; Terui, N.; Tachiiri, N.; Minakawa, K.; Matsuo, H.; Kameda, T.; Hasegawa, J.; Sambongi, Y.; Uchiyama, S.; Kobayashi, Y.; Igarashi, Y. *J. Am. Chem. Soc.* **2002**, *124*, 11574−11575.
(17) Ambler, R. P. *Biochim. Biophys. Acta* **1991**, *1058*, 42−47.
(18) Michel, L. V.; Bren, K. L. *J. Biol. Inorg. Chem.* **2008**, *13*, 837−845.

(19) Michel, L. V.; Ye, T.; Bowman, S. E. J.; Levin, B. D.; Hahn, M. A.; Russell, B. S.; Elliott, S. J.; Bren, K. L. *Biochemistry* **2007**, *46*, 11753−11760.
(20) Wen, X.; Bren, K. L. *Inorg. Chem.* **2005**, *44*, 8587−8593.
(21) Bren, K. L.; Kellogg, J. A.; Kaur, R.; Wen, X. *Inorg. Chem.* **2004**, *43*, 7934−7944.
(22) Zhong, L. H.; Wen, X.; Rabinowitz, T. M.; Russell, B. S.; Karan, E. F.; Bren, K. L. *Proc. Natl. Acad. Sci. U. S. A.* **2004**, *101*, 8637−8642.
(23) Bartalesi, I.; Bertini, I.; Hajieva, P.; Rosato, A.; Vasos, P. R. *Biochemistry* **2002**, *41*, 5112−5119.
(24) Russell, B. S.; Bren, K. L. *J. Biol. Inorg. Chem.* **2002**, *7*, 909−916.
(25) Russell, B. S.; Melenkivitz, R.; Bren, K. L. *Proc. Natl. Acad. Sci. U. S. A.* **2000**, *97*, 8312−8317.
(26) Tezcan, F. A.; Winkler, J. R.; Gray, H. B. *J. Am. Chem. Soc.* **1998**, *120*, 13383−13388.
(27) Miller, G. T.; Zhang, B.; Hardman, J. K.; Timkovich, R. *Biochemistry* **2000**, *39*, 9010−9017.
(28) Roncel, M.; Boussac, A.; Zurita, J. L.; Bottin, H.; Sugiura, M.; Kirilovsky, D.; Ortega, J. M. *J. Biol. Inorg. Chem.* **2003**, *8*, 206−216.
(29) Ikeda-Saito, M.; Prince, R. C. *J. Biol. Chem.* **1985**, *260*, 8301−8305.
(30) Battistuzzi, G.; Borsari, M.; Ranieri, A.; Sola, M. *Arch. Biochem. Biophys.* **2002**, *404*, 227−233.
(31) Battistuzzi, G.; Borsari, M.; Sola, M.; Francia, F. *Biochemistry* **1997**, *36*, 16247−16258.
(32) Battistuzzi, G.; Borsari, M.; Cowan, J. A.; Eicken, C.; Loschi, L.; Sola, M. *Biochemistry* **1999**, *38*, 5553−5562.
(33) Krishna, M. M. G.; Maity, H.; Rumbley, J. N.; Englander, S. W. *Protein Sci.* **2007**, *16*, 1946−1956.
(34) Battistuzzi, G.; Borsari, M.; Loschi, L.; Martinelli, A.; Sola, M. *Biochemistry* **1999**, *38*, 7900−7907.
(35) Trivedi, S.; Gehlot, H. S.; Rao, S. R. *Genet. Mol. Res.* **2006**, *5*, 816−827.
(36) Arai, H.; Kanbe, H.; Ishii, M.; Igarashi, Y. *J. Bacteriol.* **2010**, *192*, 2651−2652.
(37) Baltch, A. L.; Smith, R. P. *Pseudomonas aeruginosa: Infections and treatment*; Dekker: New York, 1994.
(38) Abboud, R.; Popa, R.; Souza-Egipsy, V.; Giometti, C. S.; Tollaksen, S.; Mosher, J. J.; Findlay, R. H.; Nealson, K. H. *Appl. Environ. Microbiol.* **2005**, *71*, 811−816.
(39) SL, I.; Orrenius, S. *Arch. Biochem. Biophys.* **2004**, *423*, 37−46.
(40) Belikova, N.; Vladimirov, Y.; Ospiov, A.; Kapralov, A.; Tyurin, V.; Potapovich, M.; Basova, L.; Peterson, J.; Kurnikov, I.; Kagan, V. *Biochemistry* **2006**, *45*, 4998−5009.
(41) Kagan, V.; Tyurin, V.; Jiang, F.; Tyurina, Y.; Ritov, V.; Amoscato, A.; Osipov, A.; Belikova, N.; Kapralov, A.; Kini, V.; Vlasova, I.; Zhao, Q.; Zou, M.; Di, P.; Svistunenko, D.; Kurnikov, I.; Borisenko, G. *Nat. Chem. Biol.* **2005**, *1*, 223−232.
(42) Hanske, J.; Toffey, J. R.; Morenz, A. M.; Bonilla, A. J.; Schiavoni, K. H.; Pletneva, E. V. *Proc. Natl. Acad. Sci. U. S. A.* **2012**, *109*, 125−130.
(43) Josephs, T.; Liptak, M.; Hughes, G.; Lo, A.; Smith, R.; Wilbanks, S.; Bren, K.; Ledgerwood, E. *J. Biol. Inorg. Chem.* **2013**, *18*, 289−297.